PERGAMON

International Journal of Solids and Structures 37 (2000) 7501–7528

INTERNATIONAL JOURNAL OF SOLIDS and STRUCTURES

www.elsevier.com/locate/ijsolstr

Error estimation and adaptivity for nonlocal damage models ☆

Antonio Rodríguez-Ferran *, Antonio Huerta

Departament de Matemàtica Aplicada III, E.T.S. de Ingenieros de Caminos Edifici C2, ETSECCPB, Campus Nord, Universitat Politècnica de Catalunya, E-08034 Barcelona, Spain

Received 11 November 1999; in revised form 29 March 2000

Abstract

Nonlocal damage models are typically used to model failure of quasi-brittle materials. Due to brittleness, the choice of a particular model or set of parameters can have a crucial influence on the structural response. To assess this influence, it is essential to keep finite element discretization errors under control. If not, the effect of these errors on the result of a computation could be erroneously interpreted from a constitutive viewpoint. To ensure the quality of the FE solution, an adaptive strategy based on error estimation is proposed here. It is based on the combination of a residual-type error estimator and quadrilateral *h*-remeshing. Another important consequence of brittleness is that it leads to structural responses of the snap-through or snap-back type. This requires the use of arc-length control, with a definition of the arc parameter that accounts for the localized nature of quasi-brittle failure. All these aspects are discussed for two particular nonlocal damage models (Mazars and modified von Mises) and for two tests: the Brazilian tensile splitting test and the single-edge notched beam test. For the latter test, the capability of the Mazars model to capture the curved crack pattern observed in experiments – a topic of debate in the literature – is confirmed.

Keywords: Damage models; Nonlocal models; Nonlinear problems; Error estimation; Adaptivity; Quality of FE solution

1. Introduction

Damage models are often used to model the failure of concrete and other quasi-brittle materials (Lemaitre and Chaboche, 1990). In scalar models damage is represented by a damage parameter ranging from 0 (for the virgin material with elastic stiffness) to 1 (for the completely damaged material, with no stiffness). If the damage parameter depends only on the strain state at the point under consideration, the numerical simulations exhibit a pathological mesh dependence, and physically unrealistic results are obtained. This behaviour of so-called local damage models, caused by a change of type of the governing partial differential equations, is widely reported in the literature (e.g. Bažant et al., 1984).

☆ Contract grant sponsor: Ministerio de Educación y Cultura; Contract grant number: TAP98-0421.

* Corresponding author.

E-mail address: antonio.rodriguez-ferran@upc.es

www.upc.es/ma3/lacan.html (A. Rodríguez-Ferran).

0020-7683/00/$ - see front matter
PII: S0020-7683(00)00209-2

To solve the pathological mesh dependence of local models, various regularisation techniques have been suggested (de Borst et al., 1993). One possibility is to use nonlocal damage models (Pijaudier-Cabot and Bažant, 1987; Bažant and Pijaudier-Cabot, 1988; Mazars and Pijaudier-Cabot, 1989). The basic idea of nonlocal models is that the damage parameter depends on the strain state in a neighbourhood (associated to a characteristic length) of the point under consideration. Another possibility is the use of gradient models, in which strain derivatives are incorporated in the description of damage evolution (de Borst et al., 1995). The relation between nonlocal and gradient models is discussed by Huerta and Pijaudier-Cabot (1994) and Peerlings et al. (1998).

The quasi-brittle behaviour is modelled by means of a stress–strain constitutive equation consisting of an elastic branch and a softening post-peak branch. This typically results in highly nonlinear structural responses, of the snap-through or snap-back type. Efficient nonlinear solvers based on arc-length control (Crisfield, 1991) are needed for the numerical simulations.

Due to the brittleness and high nonlinearity of the response, the particular expression of the constitutive equations or the value of the material parameters can have a major influence on the results of the computations, not only from a quantitative but also from a qualitative point of view. Indeed, as shown later with some examples, different sets of material parameters can lead to completely different failure patterns.

Of course, the finite element discretization errors also affect the results. This influence is generally of a quantitative nature. In the case of complex failure mechanisms, the finite element mesh can even have a qualitative influence on the response, as shown by Huerta and Díez (2000) and Díez et al. (2000).

Error analysis in localization problems is a field of active research in recent years. An a priori error analysis is presented in Huerta and Pijaudier-Cabot (1994) for transient problems. One of the conclusions is that the finite element size must be smaller than the characteristic length in order to avoid spurious oscillations. Moreover, an a posteriori error analysis in localization problems is already presented by Huerta et al. (1997), Arroyo et al. (1997), Huerta and Díez (2000) and Díez et al. (2000) for viscoplastic regularization of softening. Nonlocal damage models have received less attention, and they constitute the focus of this work.

In summary, two factors can have a crucial impact on the results: (1) the material modelling and (2) the numerical discretization. The main objective of this paper is to show that the FE discretization errors should be controlled if one wants to assess the behaviour of a particular damage model and/or set of parameters. If FE errors are not controlled, their effect in the solution could be erroneously attributed to the material modelling. For instance, a comparative analysis of two different damage models with a very coarse mesh (Fichant et al., 1999) can be of little significance, even at the qualitative level.

In order to control the FE discretization errors, an adaptive strategy based on error assessment for nonlocal damage models is proposed here. The adaptive strategy (Huerta et al., 1999) is based on the combination of a residual-type error estimator (Díez et al., 1998a; Huerta and Díez, 2000) and quadrilateral *h*-remeshing (Sarrate and Huerta, 2000).

An outline of paper follows. The basic features of nonlocal damage models are briefly reviewed in Section 2. Section 3 deals with the solution of the nonlinear systems of equations. The proposed adaptive strategy, including a brief review of the error estimator, is presented in Section 4. All these aspects are illustrated by means of some numerical examples in Section 5. Two tests are considered: the Brazilian cylinder-splitting test (Section 5.1) and the single-edge notched beam (Section 5.2). Finally, some concluding remarks are made in Section 6.

2. Nonlocal damage models

The basic features of nonlocal damage models are briefly reviewed in this section. First, the generic equations are presented in Section 2.1. The definition of the state variable and the evolution law for the damage parameter – the two key ingredients of a nonlocal damage model – are discussed in Sections 2.2 and

2.3 respectively. Finally, the two particular models employed in this work are summarized in Sections 2.4 (Mazars model) and 2.5 (modified von Mises model).

2.1. Generic equations

For the sake of clarity, only isotropic elastic-damage models are considered in this work. These simple models, which describe in a satisfactory manner damage due mainly to uniaxial extensions, see Fichant et al. (1999), are sufficient to illustrate the importance of adaptivity based on error estimation in damage computations. However, the approach presented here and the conclusions drawn can be extended to more complex damage models, incorporating, for instance, anisotropy and/or coupling with plasticity (Mazars and Pijaudier-Cabot, 1989), or, more generally, to any complex constitutive model.

The loss of stiffness associated to mechanical degradation of the material is represented by a parameter D, according to

$$\boldsymbol{\sigma} = (1 - D)\mathbf{C} : \boldsymbol{\varepsilon}, \tag{1}$$

where $\boldsymbol{\sigma}$ and $\boldsymbol{\varepsilon}$ are respectively the Cauchy stress tensor and the small strain tensor, and $\mathbf{C}$ is the tensor of elastic moduli (E: Young's modulus; v: Poisson's coefficient). Parameter D ranges between 0 (virgin material, with elastic stiffness) and 1 (completely damaged material, with no stiffness). It is assumed that D depends on a state variable Y, which in turn depends on the strains

$$Y = Y(\boldsymbol{\varepsilon}). \tag{2}$$

The basic idea of nonlocal damage models is averaging the state variable Y in the neighbourhood of each point. In this manner, the *nonlocal* state variable $\widetilde{Y}$ is obtained:

$$\widetilde{Y} = \int_V \alpha(d) Y \mathrm{d}V \Big/ \int_V \alpha(d) \mathrm{d}V. \tag{3}$$

The weight function α, which depends on the distance d to the point under consideration, is typically the Gaussian

$$\alpha(d) = \exp\left[-\left(\frac{2d}{l_c} \right)^2 \right], \tag{4}$$

where the characteristic length l_c is a material parameter of the nonlocal damage model. The nonlocal state variable drives the evolution of damage,

$$D = D(\widetilde{Y}). \tag{5}$$

Damage starts above a threshold Y_0 (that is, $D = 0$ for $\widetilde{Y} \leqslant Y_0$) and it cannot decrease (that is, $\dot{D} \geqslant 0$).

The characteristic length which appears in Eq. (4) acts as a localization limiter, thus regularizing the problem (Pijaudier-Cabot and Huerta, 1991). In this manner, the pathological mesh dependence of local damage models, in which damage is driven by the *local* state variable Y is avoided.

Eqs. (1)–(5) describe a generic nonlocal damage model. To define a particular model, it is necessary to specify the definition of the state variable, Eq. (2), and the evolution law for damage, Eq. (5). These two issues are addressed in the following.

2.2. Definition of the state variable

Since the state variable drives damage, Y should account for those features of the strain field which are responsible for damage inception and propagation. As discussed by Peerlings et al. (1998), Y should be

more sensitive to positive strains than to negative strains. In the Mazars model (Mazars, 1986), for instance, Y is a function of the principal strains ε_i,

$$Y = \sqrt{\sum_i [\max(0, \varepsilon_i)]^2}. \tag{6}$$

Note that only the positive principal strains are accounted for in the definition of Y.

In the modified von Mises model (de Vree et al., 1995), on the other hand, Y is defined as

$$Y = \frac{k-1}{2k(1-2\nu)} I_1 + \frac{1}{2k}\sqrt{\left(\frac{k-1}{1-2\nu} I_1\right)^2 + \frac{12k}{(1+\nu)^2} J_2}, \tag{7}$$

where k is the ratio of compressive strength to tensile strength, I_1, the first invariant of the strain tensor and J_2, the second invariant of the deviatoric strain tensor.

The main difference between the two models concerns the ratio of compressive to tensile strength (Peerlings et al., 1998), which is in the order of ten for concrete. The Mazars model yields too low values; for the modified von Mises model, on the contrary, it can be controlled by means of parameter k (in the numerical examples of Section 5, k is set to 10).

2.3. Evolution of the damage parameter

Next, a particular expression for the evolution of damage for $\widetilde{Y} > Y_0$ must be chosen. Two typical choices are the exponential law (Mazars, 1986)

$$D = 1 - \frac{Y_0(1-A)}{\widetilde{Y}} - A\exp[-B(\widetilde{Y} - Y_0)] \tag{8}$$

and the so-called polynomial law (Pijaudier-Cabot and Huerta, 1991; Askes and Sluys, 1999)

$$D = 1 - \frac{1}{1 + B(\widetilde{Y} - Y_0) + A(\widetilde{Y} - Y_0)^2}. \tag{9}$$

The meaning of the two material parameters A and B is clear in a uniaxial stress–strain curve. For a one-dimensional homogeneous strain ε, $\widetilde{Y} = Y = \varepsilon$. Combining Eqs. (8) or (9) with Eq. (1) results respectively in

$$\begin{aligned} &\sigma = E\varepsilon \quad \text{for } \varepsilon \leqslant Y_0, \\ &\sigma = EY_0(1-A) + AE\exp[-B(\varepsilon - Y_0)]\varepsilon \quad \text{for } \varepsilon > Y_0 \end{aligned} \tag{10}$$

and

$$\begin{aligned} &\sigma = E\varepsilon \quad \text{for } \varepsilon \leqslant Y_0, \\ &\sigma = \frac{E\varepsilon}{1 + B(\varepsilon - Y_0) + A(\varepsilon - Y_0)^2} \quad \text{for } \varepsilon > Y_0. \end{aligned} \tag{11}$$

The aspect of these two curves for typical values of parameters A and B is shown in Fig. 1. The elastic branch is followed by a softening post-peak branch. In both cases, parameter A is associated to the residual strength and B controls the slope of the softening branch at the peak ($\varepsilon = Y_0$).

Fig. 2 shows various stress–strain curves found in the literature. Taking an exponential evolution of damage, Eq. (8), with $A = 1$, $B = 15\,000$, $E = 23\,400$ MPa and $Y_0 = 2.6 \times 10^{-4}$ leads to a high peak stress and a very abrupt softening (Pijaudier-Cabot, 1996). With a polynomial evolution of damage, Eq. (9), and parameters $A = 0$, $B = 20\,000$, $E = 30\,000$ MPa and $Y_0 = 1.2 \times 10^{-4}$, a curve with a high residual strength is obtained (Askes and Sluys, 1999). With $E = 35\,000$ MPa, $Y_0 = 6 \times 10^{-5}$ and an exponential evolution for damage very similar to Eq. (8), Peerlings et al. (1998) obtain a rather puzzling curve, which is almost bi-

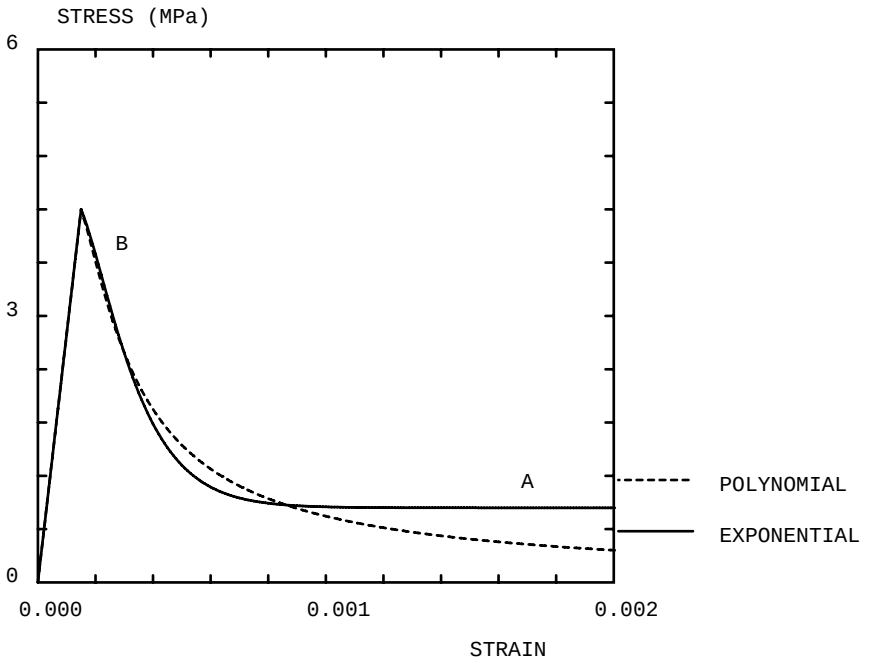

Fig. 1. One-dimensional stress–strain curves for quasi-brittle materials. For the two damage evolution laws, A is associated to the residual strength and B to the slope at the peak.

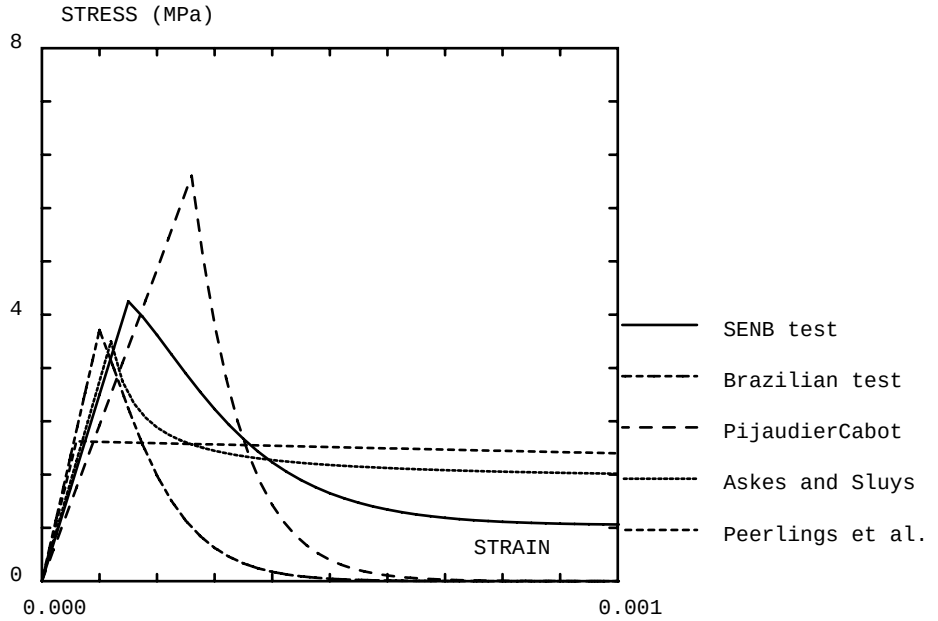

Fig. 2. Various stress–strain curves for quasi-brittle materials employed by Pijaudier-Cabot (1996), Askes and Sluys (1999) and Peerlings et al. (1998). The two curves used in Sections 5.1 (Brazilian test) and 5.2 (single-edge notched beam test) are also shown.

linear and has practically no softening. Note that, even in a quite specialized field such as scalar damage models for concrete, there is a wide variety of proposed stress–strain curves in the literature. Fig. 2 also shows the two curves used in Section 5 for the Brazilian test and the single-edge notched beam test, which are commented later.

2.4. Mazars model

The Mazars damage model combines the definition of Y of Eq. (6) and an exponential law for the evolution of damage, see Mazars (1986). Moreover, the damage parameter D is expressed as the weighted sum of tensile damage D_t and compressive damage D_c ($D = \alpha_t D_t + \alpha_c D_c$). For each of these two damage components, an exponential evolution law (with parameters A_t, B_t and A_c, B_c respectively) is assumed. The weights α_t and α_c are computed from the strain tensor $\boldsymbol{\varepsilon}$ as detailed by Pijaudier-Cabot and Mazars (1991) and Pegon and Anthoine (1994).

A simplified version of the Mazars model can also be found in the literature (Peerlings et al., 1998). The basic idea is combining directly Eqs. (6) and (8), without splitting damage into tensile and compressive components.

The equations for the full and the simplified versions of the Mazars model are summarized in Figs. 3 and 4 respectively.

State variable: $Y = \sqrt{\sum_i [\max(0, \varepsilon_i)]^2}$

Damage evolution: $D = \alpha_t D_t + \alpha_c D_c$ with

$$D_t = 1 - \frac{Y_0(1-A_t)}{\widetilde{Y}} - A_t \exp\left[-B_t\left(\widetilde{Y} - Y_0\right)\right]$$

$$D_c = 1 - \frac{Y_0(1-A_c)}{\widetilde{Y}} - A_c \exp\left[-B_c\left(\widetilde{Y} - Y_0\right)\right]$$

α_t and α_c computed as shown by Pijaudier-Cabot and Mazars (1991) and Pegon and Anthoine (1994).

Fig. 3. Full Mazars model.

State variable: $Y = \sqrt{\sum_i [\max(0, \varepsilon_i)]^2}$

Damage evolution: $D = 1 - \frac{Y_0(1-A)}{\widetilde{Y}} - A \exp\left[-B\left(\widetilde{Y} - Y_0\right)\right]$

Fig. 4. Simplified Mazars model.

State variable: $Y = \frac{k-1}{2k(1-2\nu)} I_1 + \frac{1}{2k}\sqrt{\left(\frac{k-1}{1-2\nu} I_1\right)^2 + \frac{12k}{(1+\nu)^2} J_2}$

Damage evolution: $D = 1 - \frac{1}{1+B(\tilde{Y}-Y_0)+A(\tilde{Y}-Y_0)^2}$

Fig. 5. Modified von Mises model with polynomial evolution of damage.

State variable: $Y = \frac{k-1}{2k(1-2\nu)} I_1 + \frac{1}{2k}\sqrt{\left(\frac{k-1}{1-2\nu} I_1\right)^2 + \frac{12k}{(1+\nu)^2} J_2}$

Damage evolution: $D = 1 - \frac{Y_0(1-A)}{\tilde{Y}} - A\exp\left[-B\left(\tilde{Y} - Y_0\right)\right]$

Fig. 6. Modified von Mises model with exponential evolution of damage.

2.5. Modified von Mises model

The basic feature of the modified von Mises model is the definition of the state variable given by Eq. (7), see de Vree et al. (1995). Regarding the evolution of damage, both the polynomial expression of Eq. (9) (Askes and Sluys, 1999) and an exponential expression similar to that of Eq. (8), see Peerlings et al. (1998), have been suggested in the literature.

Figs. 5 and 6 summarize the equations of the modified von Mises model with polynomial and exponential evolution of damage respectively.

3. Nonlinear solvers

The brittle behaviour associated to the stress–strain curves of Fig. 1 typically induces snap-through or snap-back responses, as illustrated in Section 5. As a consequence, arc-length control is required for solving the nonlinear systems of equations.

Another typical feature of damage models is localization. In many problems, damage localizes in relatively narrow bands. For this reason, standard arc-length techniques, such as spherical or cylindrical formulations (Crisfield, 1991), are not suitable for damage models. They provide a measure of the increment of the solution which is too "global", in contrast with the localized nature of the problem (Geers, 1999).

Alternatively, more "local" definitions of the arc-length parameter s are required. One possible choice (Pegon and Anthoine, 1994) is the maximum strain increment (Brazilian test, Section 5.1)

$$\Delta s = \max |\Delta \varepsilon_{ij}|. \tag{12}$$

Another possibility is to take one characteristic degree of freedom (or a combination of a few characteristic dof) as the arc-length parameter:

$$\Delta s = |\Delta u_{\text{characteristic}}|. \tag{13}$$

A common definition of s included in Eq. (13) are crack mouth displacements, which account for the relative displacement of the two nodes at the crack mouth. The crack-mouth sliding displacement (CMSD) is used to control the single-edge notched beam test of Section 5.2.

Another key issue in solving the nonlinear systems is the choice of a stiffness matrix. Due to nonlocality (i.e. interaction between Gauss points at different finite elements), computing consistent tangent matrices is not a straightforward task (Pijaudier-Cabot and Huerta, 1991; Pegon and Anthoine, 1994). In fact, it is necessary to take into account the nonlocal interaction between Gauss points (Jirásek, 1999). To avoid doing so, de Vree et al. (1995) and Askes and Sluys (1999) work with a "pseudo-consistent" tangent matrix, obtained by neglecting the nonlocality and computing the tangent moduli at each Gauss point. The resulting matrix is still nonsymmetric.

A different strategy is followed here (Pegon and Anthoine, 1994): a combination of secant stiffness matrices and an acceleration technique. Secant matrices, computed with the secant moduli $(1-D)\mathbf{C}$, see Eq. (1), are symmetric and positive definite, so standard symmetric solvers can be used. The acceleration technique is based on expressing the solution as a linear combination of the last few iterates and minimizing the residual. The weights are computed via a least-squares fit.

4. Error estimation and adaptivity

4.1. Why an adaptive strategy?

The numerical implications of the brittle behaviour of nonlocal damage models have been discussed in the previous section. From the viewpoint of modelling, the main consequence of brittleness is that the choice of the constitutive equation and the material parameters can have a *qualitative* influence on the results. Indeed, as illustrated in Section 5, changes in the constitutive modelling can lead to very different failure mechanisms.

Of course, the finite element mesh also affects the numerical solution. This influence is general quantitative. However, in some special cases – with complex failure mechanisms – the influence of the finite element mesh may even be *qualitative*. For instance, in the context of softening viscoplasticity, Díez et al. (2000) show that different meshes can lead to different failure mechanisms, even if the same constitutive equations and material parameters are employed. For dynamic problems, Huerta and Pijaudier-Cabot (1994), on the other hand, conclude that the element size must be smaller than the internal length of the model in order to obtain sufficient accuracy.

In summary, two factors affect quantitatively or even qualitatively the numerical computation: the model (constitutive equations and material parameters) and the numerical discretization (finite element mesh). This means that FE discretization errors should be controlled if the effect of the model is to be properly assessed. If models or sets of parameters are compared with a given mesh without controlling the discretization errors, the effect of these errors on the solution may be erroneously attributed to the different modelling. For instance, a comparative analysis of two different damage models with a coarse mesh (Fichant et al., 1999) can be of little significance, even if only qualitative information is sought.

To reduce the discretization errors, the finite element must be sufficiently fine. As shown by Díez et al. (2000), deciding whether a mesh is "sufficiently fine" or not for a given analysis is not a simple task. For this reason, and adaptive strategy is proposed in that reference and adapted here to the case of nonlocal damage models.

The adaptive strategy (Huerta et al., 1999) is based on the combination of a residual-type error estimator (Díez et al., 1998a; Huerta and Díez, 2000) and h-remeshing. The error distribution is computed with the error estimator and translated into desired element sizes with a so-called optimality criterion (Díez and Huerta, 1999). An unstructured quadrilateral mesh generator (Sarrate and Huerta, 2000) is then used to

build a mesh with the desired sizes. This iterative process stops (typically after 2–4 iterations) when the relative error of the solution is below a prescribed threshold set a priori.

4.2. The error estimator

The error estimator used in this work was first developed for linear problems (Díez et al., 1998a,b) and later extended to nonlinear problems (Huerta et al., 1998; Huerta and Díez, 2000; Díez et al., 2000). A detailed presentation an analysis can be found in these references. Here, only a brief review is given, together with some remarks specific of nonlocal damage models.

Using a mesh of characteristic size h, the finite element method provides the discrete equilibrium equation

$$\mathbf{f}_h^{\text{int}}(\mathbf{u}_h) = \mathbf{f}_h^{\text{ext}}, \tag{14}$$

where the unknown is the nodal displacement vector $\mathbf{u}_h$, $\mathbf{f}_h^{\text{int}}(\mathbf{u}_h)$ is the vector of nodal internal forces associated with $\mathbf{u}_h$ and $\mathbf{f}_h^{\text{ext}}$ is the discretized external force term.

The goal is estimating the error of the solution $\mathbf{u}_h$ of Eq. (14). Since the actual displacements are unknown, the actual error cannot be computed. However, using a much finer mesh of characteristic size $\tilde{h}$ ($\tilde{h} \ll h$), a new solution $\mathbf{u}_{\tilde{h}}$ is obtained which is much more accurate than $\mathbf{u}_h$, because the regularized nonlocal model ensures convergence as the element size goes to zero. This solution can be taken as a reference solution and, consequently, the actual error can be fairly replaced by the reference error $\mathbf{e}_{\tilde{h}}$, i.e. the difference between $\mathbf{u}_{\tilde{h}}$ and $\mathbf{u}_h$.

Note, however, that the determination of $\mathbf{u}_{\tilde{h}}$ (or $\mathbf{e}_{\tilde{h}}$) requires solving an equation analogous to Eq. (14) but in the finer mesh

$$\mathbf{f}_{\tilde{h}}^{\text{int}}(\mathbf{u}_{\tilde{h}}) = \mathbf{f}_{\tilde{h}}^{\text{int}}(\mathbf{u}_h + \mathbf{e}_{\tilde{h}}) = \mathbf{f}_{\tilde{h}}^{\text{ext}}. \tag{15}$$

This problem is computationally much more expensive than the original one. The basic idea of the error estimator is to approximate $\mathbf{e}_{\tilde{h}}$ by low-cost local computations, following the standard procedure in residual-type error estimators. That is, instead of solving Eq. (15), $\mathbf{e}_{\tilde{h}}$ is approximated by solving a set of local problems. The method consists of two phases. First, a simple residual problem is solved inside each element (interior estimation). Second, a new family of simple local problems over so-called patches is considered and the interior estimate is complemented adding a new contribution (patch estimation).

In order to simplify the presentation, the error estimator is presented for the linear case first and then extended to nonlinear problems.

4.2.1. The error estimator for linear problems

If the problem is linear, $\mathbf{f}^{\text{int}}(\mathbf{u})$ is a linear function of $\mathbf{u}$ and, consequently, Eqs. (14) and (15) become

$$\mathbf{f}_h^{\text{int}}(\mathbf{u}_h) = \mathbf{K}_h\mathbf{u}_h \quad \text{and} \quad \mathbf{f}_{\tilde{h}}^{\text{int}}(\mathbf{u}_{\tilde{h}}) = \mathbf{K}_{\tilde{h}}\mathbf{u}_{\tilde{h}}, \tag{16}$$

where $\mathbf{K}_h$ and $\mathbf{K}_{\tilde{h}}$ are the elastic stiffness matrices associated with the coarse computational mesh and the finer mesh respectively. These two equations can be easily manipulated to provide a linear equation for the reference error,

$$\mathbf{K}_{\tilde{h}}\mathbf{e}_{\tilde{h}} = \mathbf{f}_{\tilde{h}}^{\text{ext}} - \mathbf{f}_{\tilde{h}}^{\text{int}}(\mathbf{u}_h) =: -\mathbf{r}_{\tilde{h}}(\mathbf{u}_h), \tag{17}$$

where $\mathbf{f}_{\tilde{h}}^{\text{int}}(\mathbf{u}_h)$ is the internal force vector in the finer mesh associated with the solution $\mathbf{u}_h$ of the coarse mesh, and $\mathbf{r}_{\tilde{h}}(\mathbf{u}_h)$ is the residual.

Fig. 7 shows a graphic illustration of the reference error and its relation with the residual. The solutions $\mathbf{u}_h$ and $\mathbf{u}_{\tilde{h}}$ can be seen as the intersection between the curves describing the evolution of the internal forces

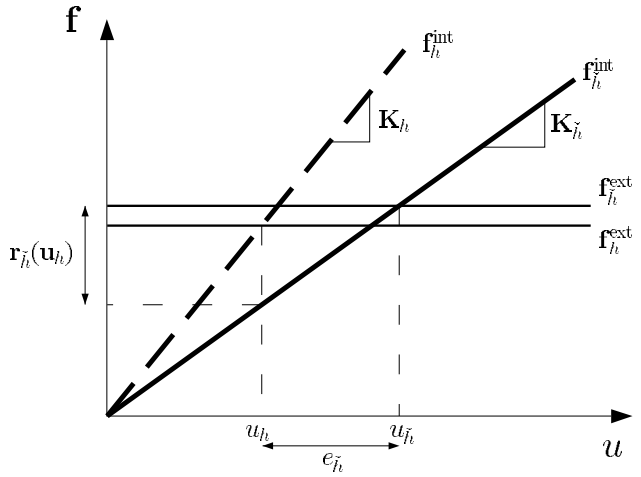

Fig. 7. Graphic interpretation of the reference error in linear problems.

and the horizontal lines corresponding to the discretized external forces (which are assumed to be independent of the solution). In the linear case the evolution of internal forces is described by straight lines and everything turns trivial.

It is clear from Fig. 7 that the reference error, $\mathbf{e}_{\tilde{h}} = \mathbf{u}_{\tilde{h}} - \mathbf{u}_h$, and the residual, $\mathbf{r}_{\tilde{h}}(\mathbf{u}_h) := \mathbf{f}_{\tilde{h}}^{\text{int}}(\mathbf{u}_h) - \mathbf{f}_{\tilde{h}}^{\text{ext}}$, are indeed related by the stiffness matrix in the reference mesh, $\mathbf{K}_{\tilde{h}}$, as indicated by Eq. (17).

4.2.1.1. Interior estimation. The finer reference mesh is constructed by assembling submeshes over each element. These elementary submeshes are built by mapping a submesh over the reference element into the elements of the actual mesh, see Fig. 8.

To avoid unaffordable computations (notice that Eq. (17) is a very large system of equations), the error estimation must be performed solving local problems. This is standard in residual-type error estimators. The natural partition of the domain to define these local problems is the set of elements of the "coarse" computational mesh (denoted by Ω_k, $k = 1, \ldots$).

The elementary submeshes of Fig. 8 can be used to solve the error Eq. (17) on each element Ω_k of the original mesh. The solution of such problems requires of course proper boundary conditions for the error. Most residual-type error estimators use an involved and expensive flux-splitting procedure to prescribe the error flux around each element Ω_k. In contrast with this common approach, the estimator used in this work

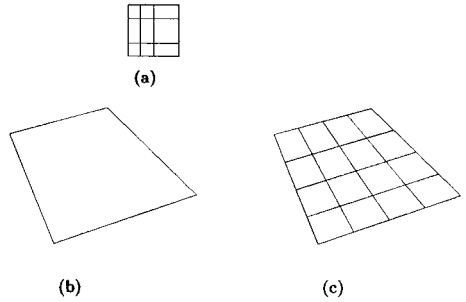

Fig. 8. (a) The reference submesh is mapped into (b) an element to get (c) an elementary submesh.

avoids complex boundary conditions: trivial (homogeneous Dirichlet) boundary conditions are imposed for both sets of local problems. This feature is probably its major advantage with respect to other residual-type estimators. The consequences of such a choice for the boundary conditions are discussed later.

Thus, the interior estimation consists of solving Eq. (17) at element level and prescribing the error in displacements to be zero in all the boundary nodes of the elementary submesh. This results in the system of equations

$$\mathbf{K}_k^{\mathrm{e}}\boldsymbol{\varepsilon}_k = -\mathbf{r}_k^{\mathrm{e}}, \tag{18}$$

where $\mathbf{K}_k^{\mathrm{e}}$ is the local stiffness matrix associated with the elementary submesh over element Ω_k and $\mathbf{r}_k^{\mathrm{e}}$ is the restriction of the residual to this element. The vector $\boldsymbol{\varepsilon}_k$ is an approximation to the restriction of the reference error $\mathbf{e}_{\tilde{h}}$ inside the element Ω_k. In the linear case, the squared local energy norm of the interior estimate $\boldsymbol{\varepsilon}_k$ can be directly computed as

$$\|\boldsymbol{\varepsilon}_k\|^2 = \boldsymbol{\varepsilon}_k^{\mathrm{T}}\mathbf{K}_k^{\mathrm{e}}\boldsymbol{\varepsilon}_k = -\boldsymbol{\varepsilon}_k^{\mathrm{T}}\mathbf{r}_k^{\mathrm{e}}. \tag{19}$$

Once the elementary problems are solved, the local interior estimates can be assembled to build up a global estimate $\boldsymbol{\varepsilon}$ over the whole domain Ω,

$$\boldsymbol{\varepsilon} = \sum_k \boldsymbol{\varepsilon}_k. \tag{20}$$

The global norm of $\boldsymbol{\varepsilon}$ can be easily computed using the local estimates as

$$\|\boldsymbol{\varepsilon}\|^2 = \sum_k \|\boldsymbol{\varepsilon}_k\|^2. \tag{21}$$

The choice of homogeneous Dirichlet boundary condition implies that $\|\boldsymbol{\varepsilon}\| \ll \|\mathbf{e}_{\tilde{h}}\|$. The reference error $\mathbf{e}_{\tilde{h}}$ is, most probably, non-zero along the element edges, thus $\boldsymbol{\varepsilon}$ may be a poor approximation to $\mathbf{e}_{\tilde{h}}$. This fact is taken into account in the patch estimation.

4.2.1.2. Patch estimation and complete estimate. Once the interior estimate is computed, it is necessary to improve the error estimation by adding nonzero values in the element boundaries. This can be done following the same idea of the interior estimation, precluding the direct computation of flux jumps and avoiding any flux splitting procedure.

The interior estimate is based on solving local problems in the elements, the natural partition of the domain Ω. In this second phase, a different set of subdomains, called patches, is considered. Each patch is associated to a node and covers one-fourth of each element sharing that node, see Fig. 9.

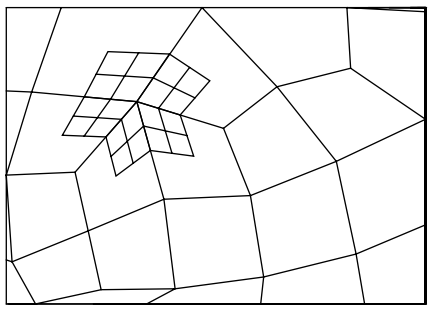

Fig. 9. Patch submesh centred in a node of the computational mesh.

The idea is to use this new partition to define new local problems – with the help of a submesh – for the error. Again, homogeneous Dirichlet boundary conditions are imposed on the whole boundary of each patch. A system analogous to that of Eq. (18) must be solved for each patch. In this manner, a new approximation to the error is obtained. The key idea of the patch estimation is that this new approximation takes nonzero values in the boundary of the elements, where the interior estimate ε vanishes. Thus, flux jumps across element edges are accounted for.

Using the patch estimation, local and global error estimates can be computed following equations analogous to Eqs. (19) and (21) respectively. Care is taken during patch estimation to ensure orthogonality between the patch estimate and the interior estimate. By doing so, the two contributions can be added and a new approximation to the reference error is found.

4.2.2. The error estimator for nonlinear problems

If the problem is nonlinear, Eq. (17) does not hold and the only available equation for the error is Eq. (15). That is, the reference error $\mathbf{e}_{\tilde{h}}$ verifies

$$\mathbf{f}^{\text{int}}_{\tilde{h}}(\mathbf{u}_h + \mathbf{e}_{\tilde{h}}) = \mathbf{f}^{\text{ext}}_{\tilde{h}}. \tag{22}$$

This is a general nonlinear equation, to be solved using any standard nonlinear solver. In fact, this problem is equivalent to finding the reference solution $\mathbf{u}_{\tilde{h}}$ (recall that $\mathbf{u}_{\tilde{h}} = \mathbf{u}_h + \mathbf{e}_{\tilde{h}}$). Note, however, that the unknown $\mathbf{e}_{\tilde{h}}$ can be assumed to be small compared with $\mathbf{u}_{\tilde{h}}$ and, consequently, this nonlinear problem is much easier than the original one (because $\mathbf{u}_h$ is a good initial approximation to $\mathbf{u}_{\tilde{h}}$). Typically only two iterations are needed for convergence. Fig. 10 illustrates the nonlinear error estimation. Note that, in contrast to Fig. 7, the curves describing the evolution of the internal forces are not straight lines due to nonlinearity, so an iterative solver is needed to compute $\mathbf{e}_{\tilde{h}}$.

If the tangent stiffness matrix is available, this general nonlinear estimation can be simplified by means of a standard linearization (Huerta and Díez, 2000; Díez et al., 2000). The resulting tangent error estimation is illustrated in Fig. 11. The reference error is approximated using a tangent approximation of the curve representing the behaviour associated with the finer mesh. However, as discussed in Section 3, computing

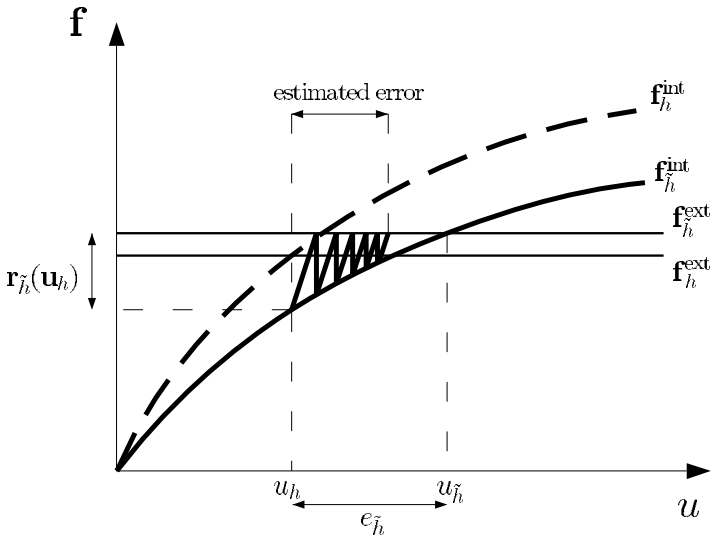

Fig. 10. Graphic interpretation of the reference error in nonlinear problems and fully nonlinear error estimation.

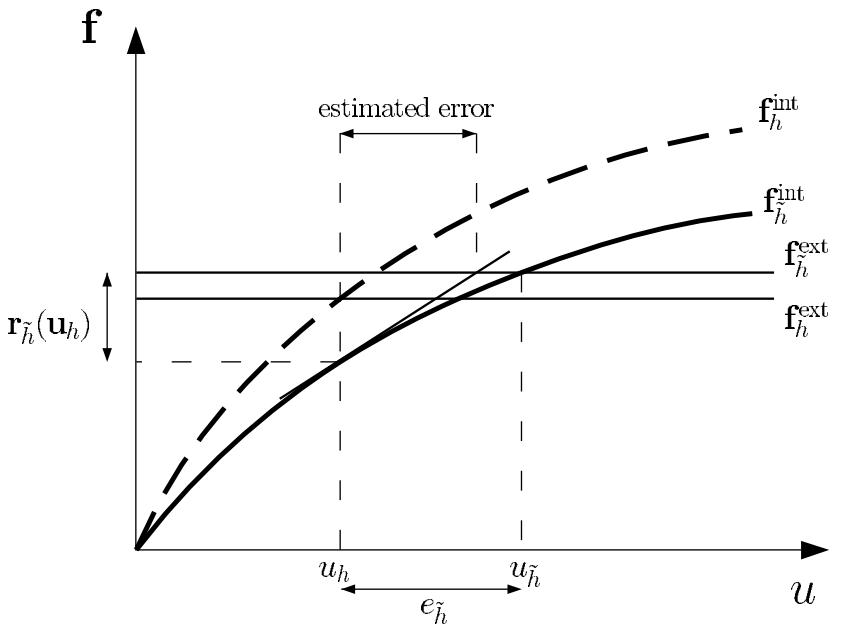

Fig. 11. Graphic interpretation of the reference error in nonlinear problems and error estimation using tangent approximation.

tangent stiffness matrices is involved for nonlocal damage models, so they are not used in this work. In fact, the nonlinear error estimation is performed iteratively as shown in Fig. 10, by means of the same combination of secant stiffness matrices and acceleration technique used to compute the solution.

The main idea of the generalization of the error estimator to nonlinear cases is to reproduce the same structure of the linear case with a different equation for the error. Thus, again in this case, the estimation of the error is splitted into two steps. First, elementary nonlinear problems are solved over the elements with null error boundary conditions, and an interior estimate is computed. Second, a nonlinear problem is solved over each patch, again with homogeneous Dirichlet boundary conditions. Once the two contributions are added, the energy of the error is measured using a simple scalar product: $\|\varepsilon_k\|^2 = -\varepsilon_k^{\mathrm{T}}\mathbf{r}_k^{\mathrm{e}}$. A relative error is obtained (see Section 5.2) by dividing the energy of the error over the energy of the solution.

4.2.3. The error estimator for nonlocal damage models

To sum up, the basic idea of the error estimator is to solve local problems over the elements and over patches (with patch size $\approx$ element size, see Fig. 9). In the context of nonlocal damage models, it is important to notice that, upon mesh refinement during the adaptive process, the element/patch size may become much smaller than the characteristic length l_c of the nonlocal model. This result was already predicted by Huerta and Pijaudier-Cabot (1994) via an analytical study. As a consequence, the Gaussian function used for the nonlocal averaging, Eq. (4), is truncated and its support is limited to one element/patch. This means that, for every local problem, the nonlocal interaction between Gauss points located at different elements/patches is neglected. Since the patches overlap the elements, the current error estimation procedure (i.e. a loop of elements followed by a loop on patches) takes into account the nonlocal interaction between adjacent elements, but not between more distant elements. The development of an estimation procedure that takes into account the full nonlocality is currently under progress. Nevertheless, it should be pointed out here that the influence at a given Gauss point of distant Gauss points, which in fact recalls the concept of pollution errors, can be assessed with a global analysis (Huerta and Díez, 2000).

5. Numerical examples

The various aspects discussed in the previous sections are illustrated here by means of some numerical examples. Some basic features of nonlocal damage models are discussed in Section 5.1 for the Brazilian test. The single-edge notched beam is considered in Section 5.2, where emphasis is put on the proposed adaptive strategy.

5.1. Brazilian test

The Brazilian splitting test is a standard technique to determine the tensile strength of concrete, rocks and other geomaterials. A cylindrical specimen is loaded along a diametral plane by means of steel bearing plates, see Fig. 12. A plane strain simulation is carried out with the full Mazars model, see Fig. 3, for the concrete specimen. Elastic behaviour is assumed for the steel bearing plates. The material parameters are shown in Table 1. As discussed by Rocco et al. (1999), the mechanism of rupture is affected by various factors, notably the ratio between the specimen radius R and the bearing plate width B. A numerical study of the influence of these parameters is not attempted here. Fixed values of $R = 40$ mm and $B = 10$ mm are considered.

Due to double symmetry, the computational domain consists of only one quarter of the specimen. Two finite element meshes, with a different element density in the zone of interest, have been used, see Fig. 13.

The nonlinear problem is solved incrementally with arc-length control, by using the maximum increment of strain as arc parameter, see Eq. (12). The highly nonlinear structural response is depicted in Fig. 14. In Fig. 14(a), the applied force (per unit height of the cylindrical specimen and over a width $B/2$) is plotted versus the vertical displacement of the bearing plate. Note the severe snap-back after the peak load is

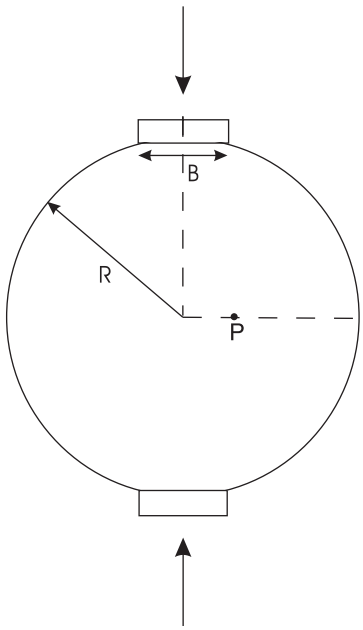

Fig. 12. Brazilian test: problem statement.

Table 1
Brazilian test. Material parameters for concrete specimen (full Mazars model) and steel bearing plates (elastic)

Parameter	Concrete	Steel
E	37700 MPa	300000 MPa
v	0.2	0.2
Y_0	10^{-4}	
A_t	1	
B_t	15600	
A_c	1.4	
B_c	1900	
l_c	5 mm	

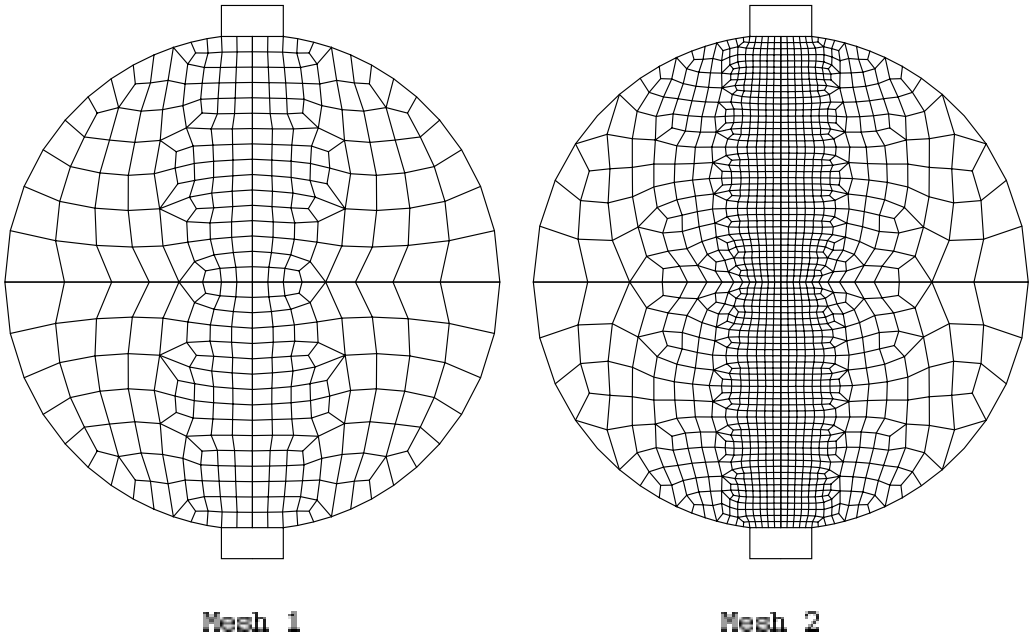

Fig. 13. Brazilian test. Two meshes (shown for the full, not the computational, domain for illustrative purposes) with different element density in the loading plane are used.

reached. Fig. 14(b), on the other hand, shows the applied force versus a measure of the crack opening displacement (the horizontal displacement of point P located under the corner of the plate, see Fig. 12).

It is interesting to note a certain amount of reloading after the minimum load is reached (from state C to state D). This behaviour is in qualitative agreement with the observations of Rocco et al. (1999) and Carmona et al. (1998). Their interpretation is illustrated here with the help of Fig. 15, where the damage field is plotted at states A, B, C and D marked in Fig. 14. Damage initiates at the centre of the specimen (state A) and propagates along the loading plane (state B) until it reaches the bearing plates (state C). This evolution of damage has been observed in experiments based on holographic interferometry (Castro-Montero et al., 1995). State C corresponds to the splitting of the disc into two half-discs. After that, there is some extra loading capacity of the two half-discs working separately under compression. Failure at state D can be associated to the formation of wedges under the bearing plates.

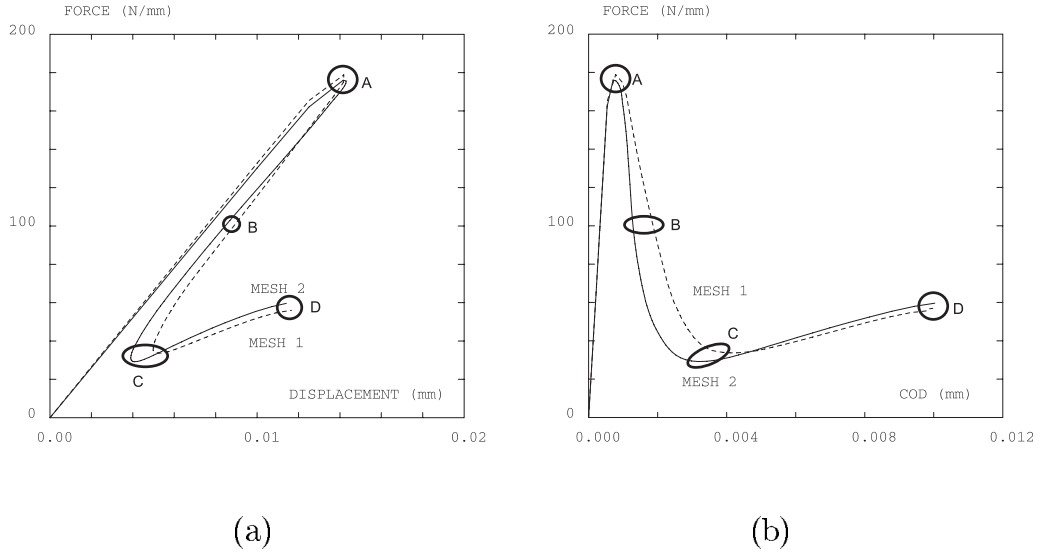

Fig. 14. Brazilian test. Force versus (a) the vertical displacement of the bearing plate and (b) the crack opening displacement (i.e. the horizontal displacement of point P, see Fig. 12). The damage field at states A, B, C and D is depicted in Fig. 15.

5.2. Single-edge notched beam

The second example is the single-edge notched beam test. First, the reference test is presented and the adaptive procedure is discussed in detail in Section 5.2.1. After that, the influence of the constitutive model and/or the material parameters is assessed in Sections 5.2.2–5.2.4.

5.2.1. Reference test

A single-edged notched beam (SENB) is subjected to an anti-symmetrical four-point loading. The geometry, loads and supports, shown in Fig. 16, correspond to the medium-size specimen tested by Carpinteri et al. (1993). A plane stress analysis is performed. To begin with, the test is carried out with the modified von Mises model with exponential damage evolution, see Fig. 6, and the material parameters of Table 2. Later in this same section, the test is reproduced with the Mazars model. The CMSD – that is, the relative vertical displacement between the two nodes at the crack mouth – is taken as the arc parameter in the arc-length control procedure.

The adaptive analysis starts with a rather coarse mesh, see Fig. 17(a), with 659 elements and 719 nodes. Note, in particular, that there is only one finite element in the notch width. This mesh is denoted `Mesh 0` to emphasize that it is the initial approximation in an iterative process. The damage distribution and the deformed mesh (amplified 300 times) for the final state (corresponding to a CMSD of 0.08 mm) are shown respectively in Fig. 17(b) and (c).

The distribution of absolute error in the final state is depicted in Fig. 17(d). The estimator clearly detects the zones with larger errors: the supports and the *edges* of the "crack" (i.e. the damaged band). The solution with `Mesh 0` has a global relative error of 4.41%, larger than the prescribed goal of 2%.

The error distribution of Fig. 17(d) and the error goal of 2% are translated into a field of desired element sizes, from which `Mesh 1` (3185 elements and 3340 nodes) is generated, see Fig. 18(a). As expected, elements are concentrated where the solution with `Mesh 0` has larger errors. With the new mesh, the damage distribution and the deformed mesh of Fig. 18(b) and (c) are obtained. Fig. 18(d) shows that there is a sig-

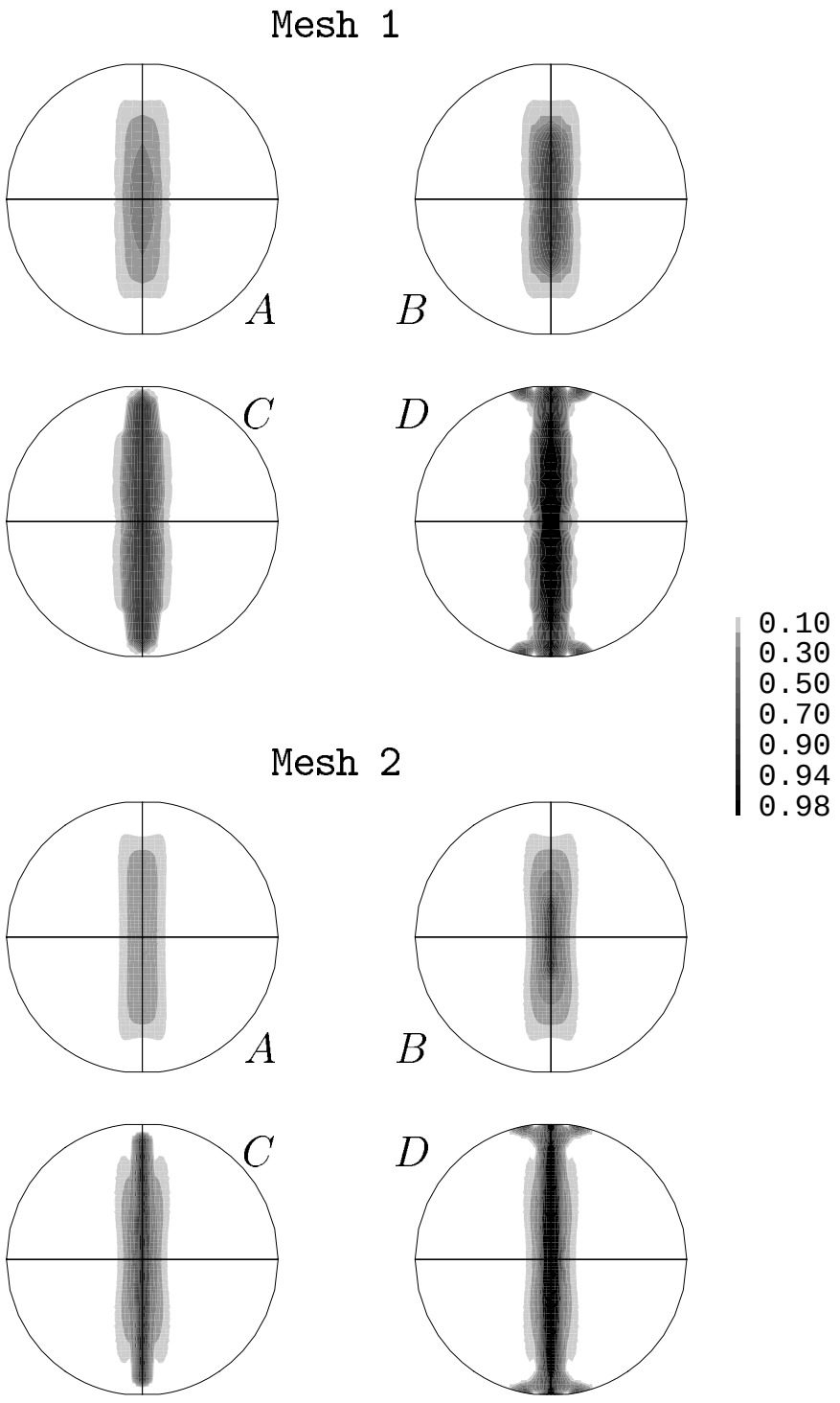

Fig. 15. Brazilian test. Evolution of the damage field for `Mesh 1` (top) and `Mesh 2` (bottom). Damage initiates at the centre of the specimen and propagates along the loading plane. States A, B, C and D are defined in Fig. 14.

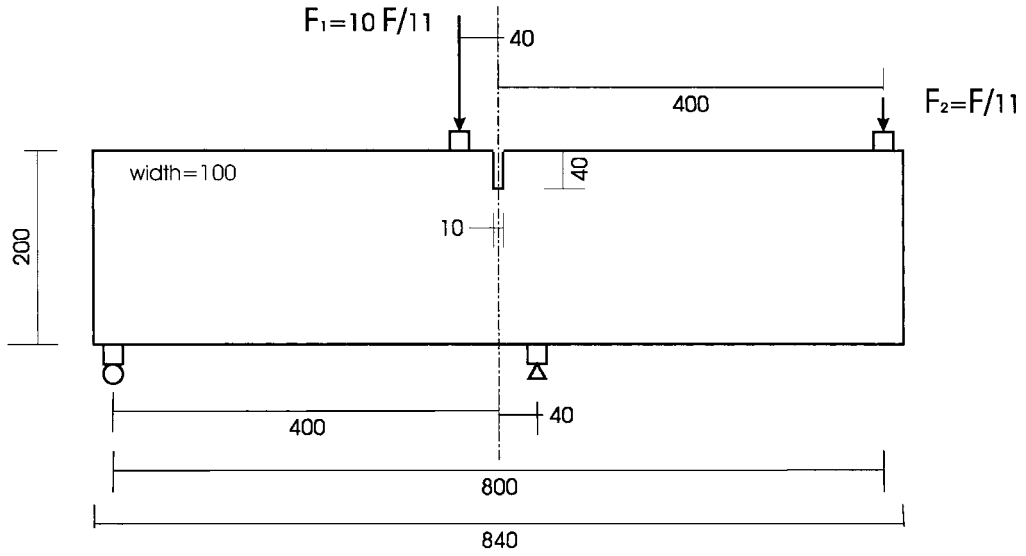

Fig. 16. Single-edge notched beam: problem statement. All distances in mm.

Table 2
SENB reference test. Material parameters for concrete beam (modified von Mises model with exponential damage evolution) and steel loading plates (elastic)

Parameter	Concrete	Steel
E	28000 MPa	280000 MPa
ν	0.1	0.2
Y_0	1.5×10^{-4}	
A	0.8	
B	9000	
l_c	10 mm	

nificant reduction in the error (note that the scale is different from that of Fig. 17(d)). The global relative error is 2.55%.

Since the goal of 2% error is still not attained, the adaptive process goes on. `Mesh 2`, with 3924 elements and 4107 nodes, is obtained, see Fig. 19(a). Note that the zones around the outermost supports have been derefined, while the edges of the crack have been refined. Fig. 19(b)–(d) show respectively the final damage distribution, deformed mesh and error field. The global relative error is 1.62%, so the solution with `Mesh 2` is acceptable and the iterative adaptive procedure is stopped.

A closer look at the adaptive process is offered by Fig. 20, which zooms on the central part of the beam. It is clear in this figure that the remeshing is indeed driven by the error field. It is also worth mentioning that errors are large in the *edges* of the crack, not in the crack itself. This result is corroborated by Fig. 21, where profiles of the damage and error fields across the crack are plotted. For the three meshes, two error peaks are found in the fronts of the damage profile. The error in the interior of the crack, on the other hand, is relatively small. This strongly suggests that damage gradient, rather than damage itself, would be a proper error indicator (Huerta et al., 1999) for this problem. A similar result is reported by Arroyo et al. (1997) in the context of softening viscoplasticity, where the gradient of inelastic strains also turns out to be a better error indicator than inelastic strains themselves. The SENB reference test just discussed has also been

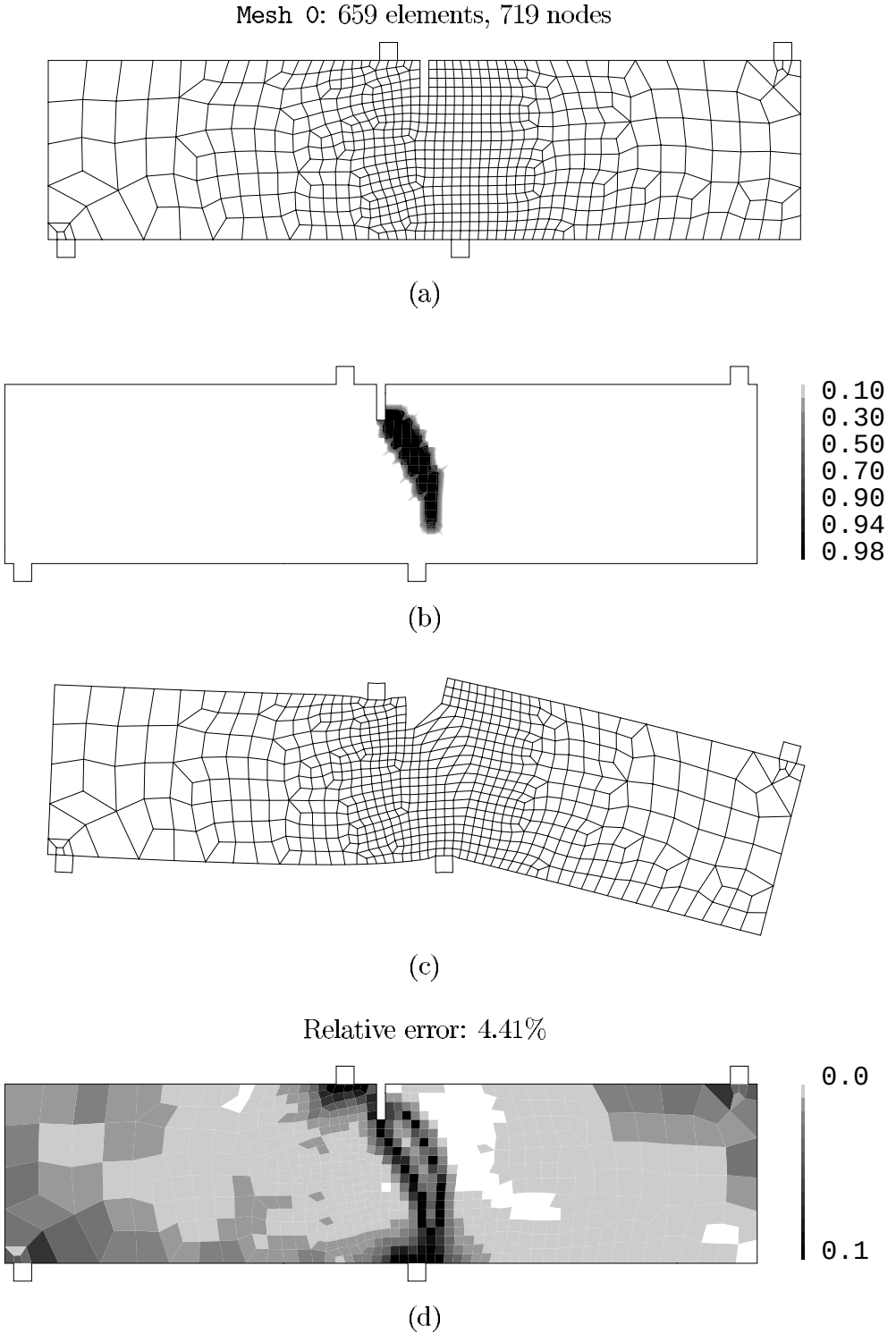

Fig. 17. SENB reference test, initial approximation in the adaptive process. (a) Mesh 0, (b) final damage distribution, (c) final deformed mesh ($\times 300$) and (d) error distribution.

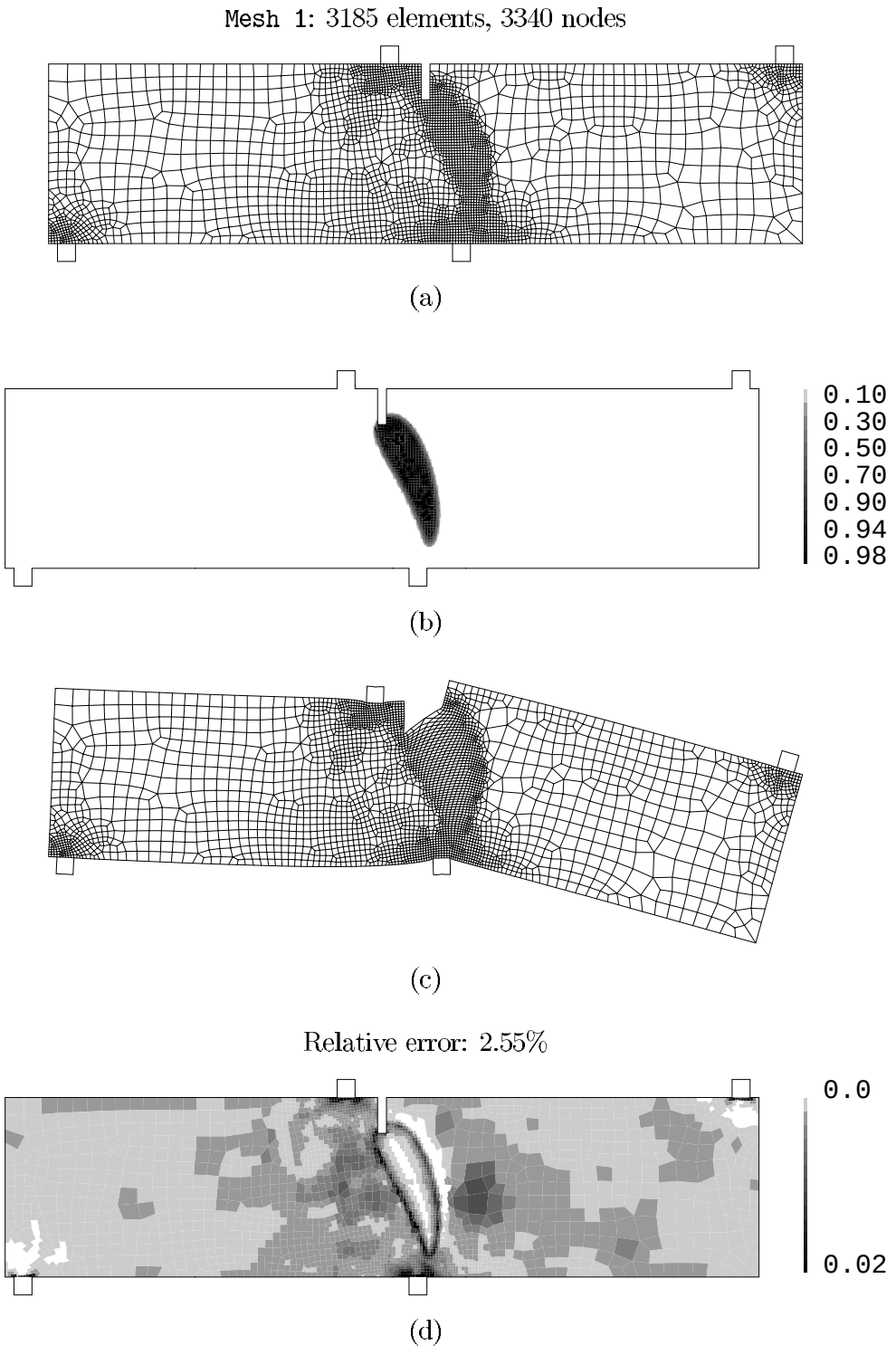

Fig. 18. SENB reference test, after one iteration in the adaptive process. (a) `Mesh 1`, (b) final damage distribution, (c) final deformed mesh (×300) and (d) error distribution.

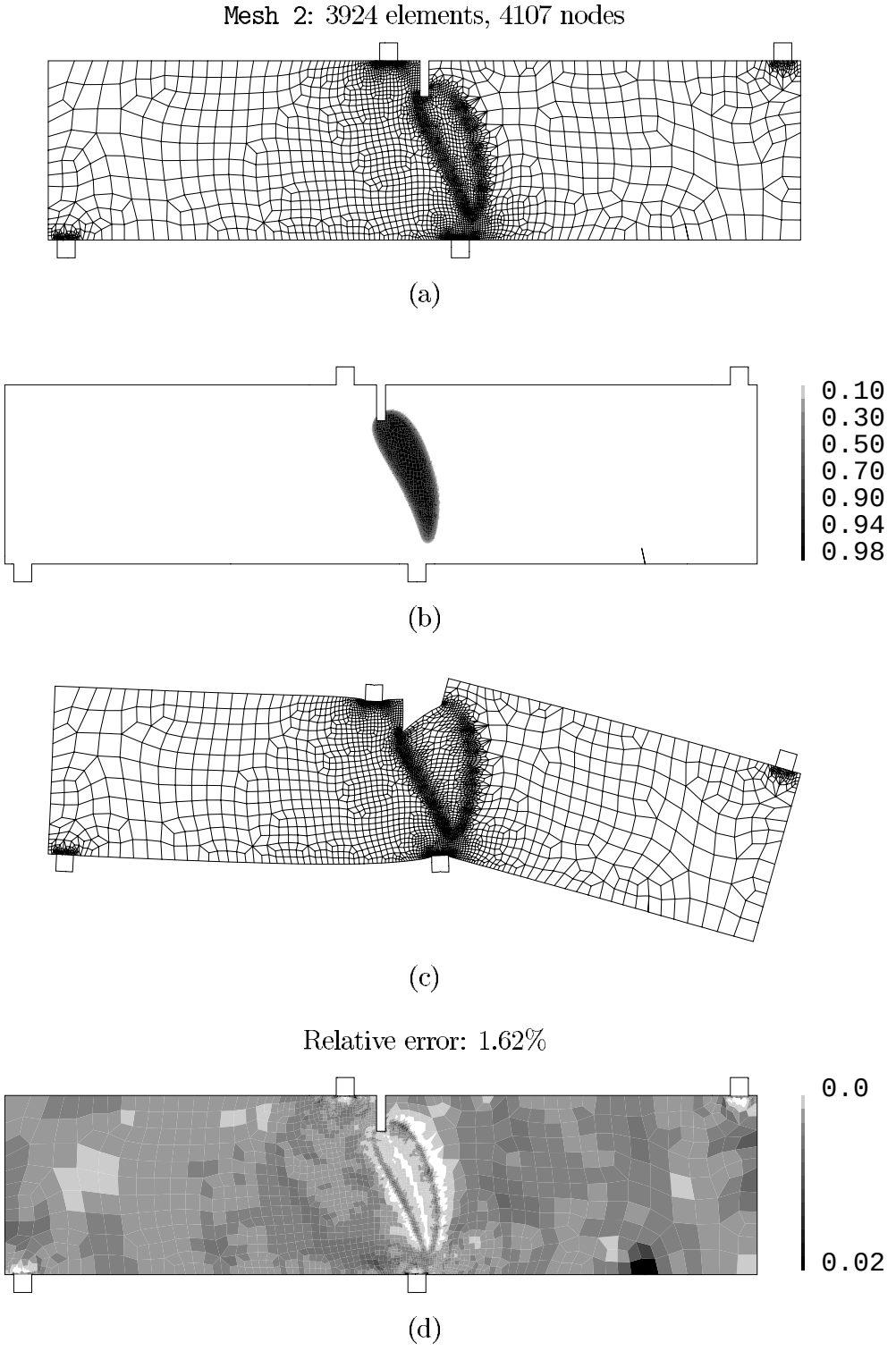

Fig. 19. SENB reference test, after two iterations in the adaptive process. (a) Mesh 2, (b) final damage distribution, (c) final deformed mesh ($\times 300$) and (d) error distribution.

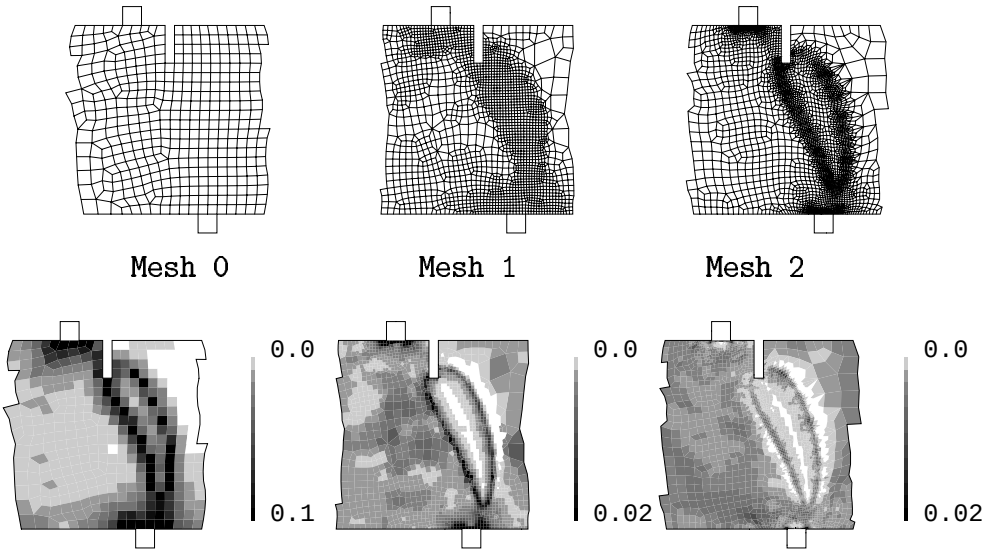

Fig. 20. SENB reference test. Zoom on the central part of the beam of the mesh (top row) and the error field (bottom row).

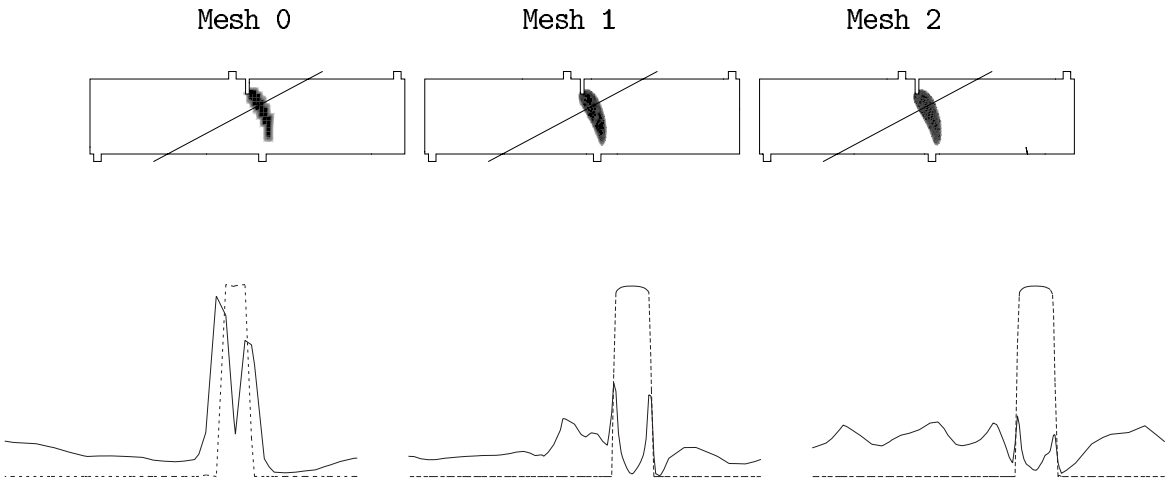

Fig. 21. SENB reference test. Profiles of damage (- - -) and error (—) across the crack. The two error peaks are associated to large damage gradients.

analyzed with the Mazars model using the material parameters of Table 2. Both the simplified version and the full version (with $A_t = A$, $B_t = B$, $A_c = 1.4$ and $B_c = 1900$) of the Mazars model, Figs. 4 and 3, have been tested. Very similar results are obtained, so it is concluded that the split of damage into tensile and compressive components is not of relevance for this test. The results are summarized in Fig. 22, showing the final damage fields obtained with `Mesh 0` and `Mesh 2`.

Figs. 18, 19 and 22 (bottom) clearly illustrate that both the modified von Mises model and the Mazars model are capable of capturing the curved crack observed in the experiments (Carpinteri et al., 1993), if a sufficiently fine mesh is employed. As discussed by Fichant et al. (1999), damage in the SENB test is es-

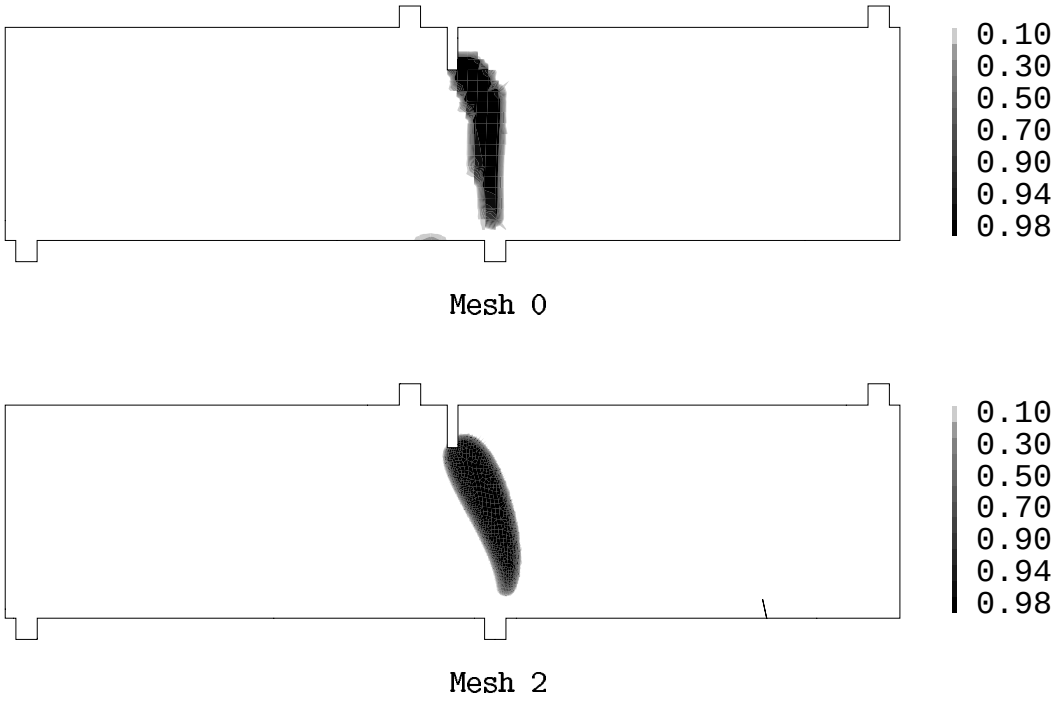

Fig. 22. SENB reference test with the Mazars model. Final damage fields obtained with `Mesh 0` and `Mesh 2`.

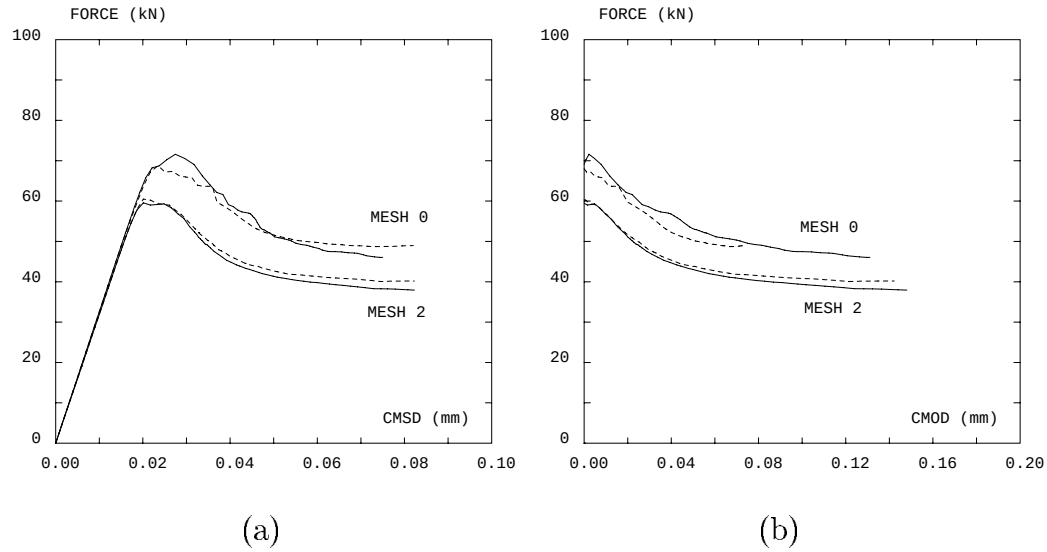

Fig. 23. SENB reference test. Total applied force F versus (a) the CMSD and (b) the crack-mouth opening displacement (CMOD). Similar results are obtained with the modified von Mises model (—) and the Mazars model (- - -).

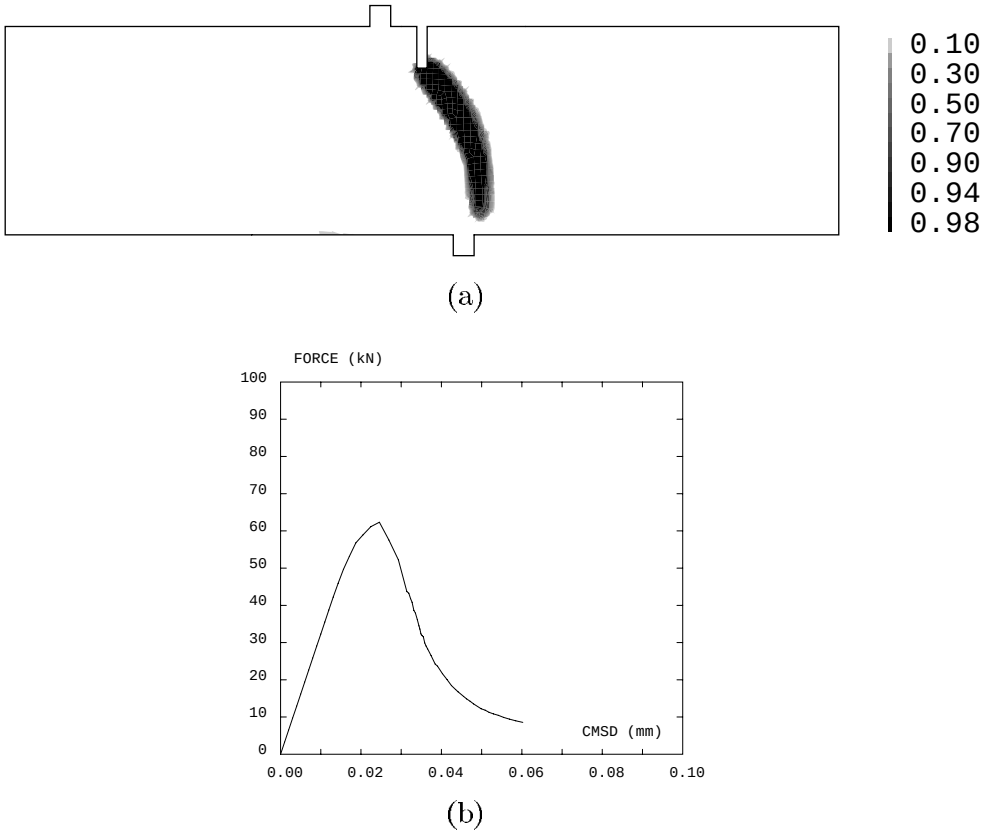

Fig. 24. SENB test. Modified von Mises model with a polynomial law for damage: (a) the final damage distribution is similar to the reference test with an exponential law (cf. Fig. 19); (b) the post-peak softening is more abrupt (cf. Fig. 23).

sentially caused by extensions. The two models yield similar results because they have the same response in uniaxial tension. The fact that the Mazars model underestimates the compressive strength has little effect, because compressive stresses play a minor role in this test.

The structural response is shown in Fig. 23. The total applied force F is plotted versus the CMSD and the CMOD (that is, relative horizontal displacement of the two nodes at the crack mouth) for the two models. There is a good qualitative and quantitative agreement with the experimental observations of Carpinteri et al. (1993), including a peak load of 60 kN and a mild softening branch after the peak load.

5.2.2. Influence of evolution law for damage

The influence of the evolution law for damage is assessed in this section. A polynomial (instead of an exponential) law is assumed for the modified von Mises model, see Fig. 5, with parameter $A = 4 \times 10^7$ and all the other parameters taken from Table 2. The two stress–strain curves (i.e. with exponential and polynomial damage evolution) are those used in Fig. 1 to illustrate the basic features of quasi-brittle response. The results are shown in Fig. 24. The final damage distribution, depicted in Fig. 24(a), is similar to that of the reference test. However, the curve F–CMSD shows a larger post-peak slope, see Fig. 24(b). This is associated to the shape of the softening branch, Fig. 1. With the exponential evolution law, a constant

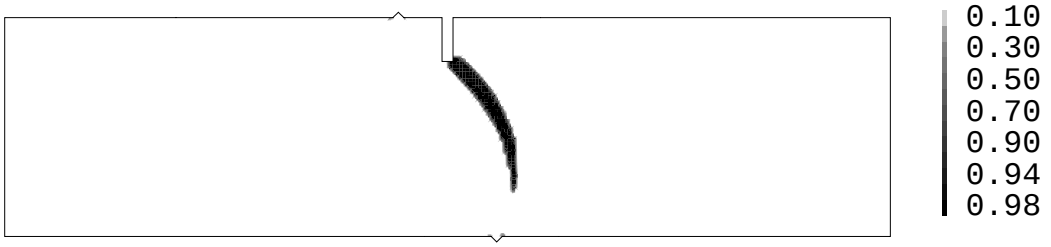

(a)

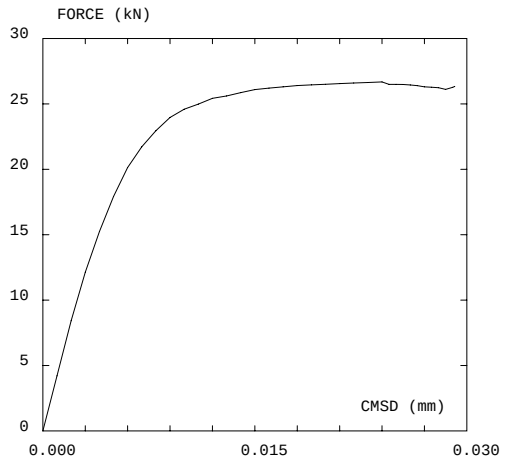

(b)

Fig. 25. SENB test of Askes and Sluys (1999). (a) The damage band is thinner because a smaller characteristic length is used. (b) The large residual strength leads to a F–CMSD curve with no softening.

residual strength is attained relatively soon; with the polynomial law, on the other hand, it decreases progressively.

5.2.3. Influence of the residual strength

The SENB test of Askes and Sluys (1999) is reproduced here. The main differences with respect to the reference test are (1) a smaller beam, (2) a lower characteristic length ($l_c = 1$ mm) and (3) a different strain–stress curve with a higher residual strength, see Fig. 2.

The results are depicted in Fig. 25. The curved crack is captured correctly, see Fig. 25(a). Note that the use of a smaller characteristic length leads to a thinner damage band. On the other hand, the large residual strength results in a structural response with no softening, see Fig. 25(b).

5.2.4. Influence of the post-peak slope

As a last test, the effect of the post-peak slope is assessed. The stress–strain curve proposed by Pijaudier-Cabot (1996), see Fig. 2, is combined with the Mazars model.

The high brittleness of the stress–strain curve affects qualitatively the results. As shown by Fig. 26(b), the structural response is very brittle and the CMSD does not increase monotonically. The final damage field of

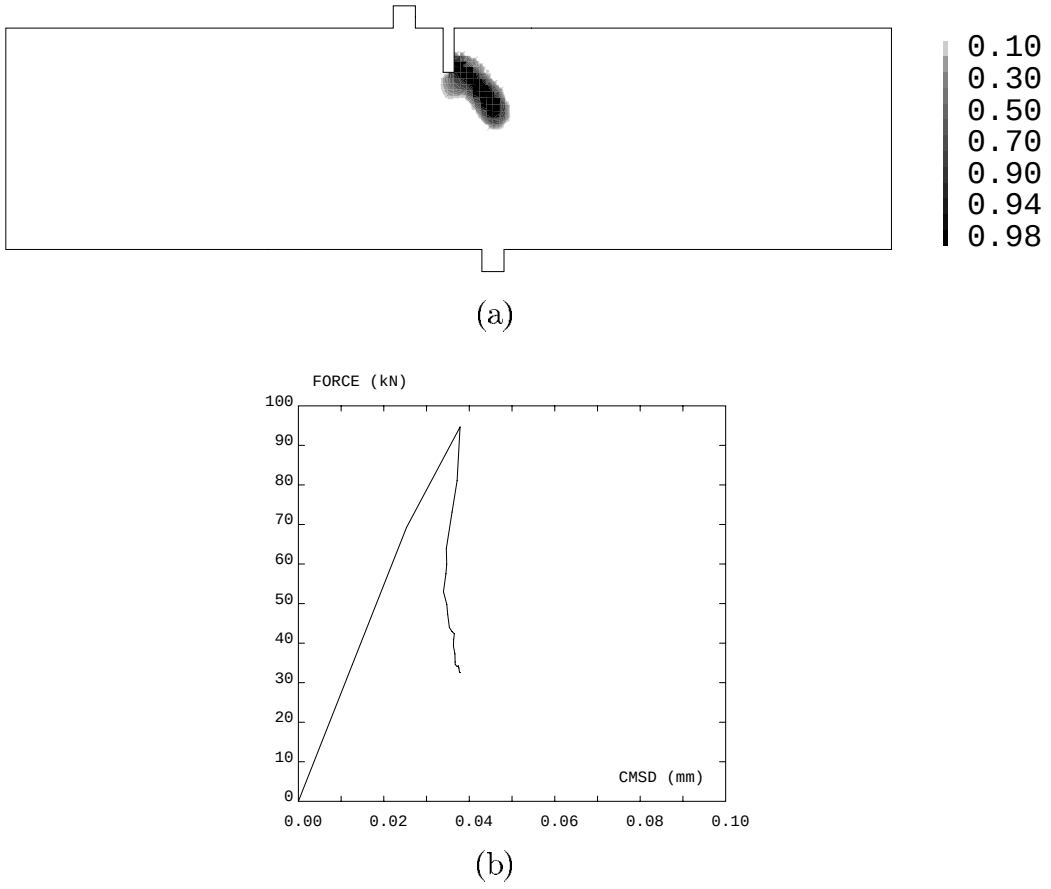

Fig. 26. SENB test of Pijaudier-Cabot (1996). The very brittle stress–strain curve results in (a) a different damage field and (b) a F–CMSD curve with snap-back.

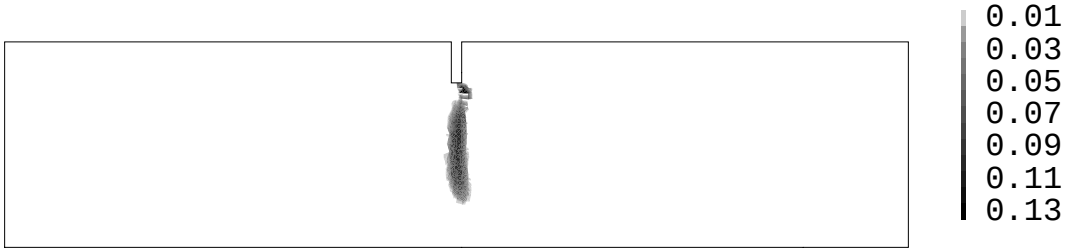

Fig. 27. SENB test with the Mazars model. For a brittle stress–strain curve and a large characteristic length, a vertical crack is obtained.

Fig. 26(a) shows that the primary crack is accompanied by what appears to be the inception of a secondary crack, right below the notch tip.

If, in addition, a larger characteristic length ($l_c = 25$ mm) and a smaller beam are considered (Schlangen, 1993), then a vertical straight crack is obtained, see Fig. 27. In fact, a comparison of Figs. 26 and 27

suggests that the incipient secondary crack of the previous test has become dominant and determines the failure pattern. A similar result (i.e. vertical straight instead of curved crack) is reported for the Mazars model by Peerlings et al. (1998). From the discussion of Section 5.2.1, it is clear that this result is due to a (not unique) particular choice of parameters, not to any intrinsic difficulty of the Mazars model to capture the curved crack of the SENB test.

6. Concluding remarks

An adaptive strategy to ensure the quality of finite element computations with nonlocal damage models has been presented. The proposed strategy relies on two basic ingredients: a residual-type error estimator and an unstructured quadrilateral mesh generator.

The constitutive modelling of failure in concrete is a topic of current research. As pointed out in this paper, there is no unanimous agreement on the stress–strain behaviour of concrete, even for the specific case of scalar nonlocal elastic-damage models.

A key issue in the nonlinear solution of complex damage problems is the use of local control variables, which take into account the localized nature of the failure pattern.

The error estimator is probably the most distinct feature of the proposed adaptive strategy. An existing residual-type nonlinear error estimator has been extended to the context of nonlocal damage models, where tangent stiffness matrices are not readily available.

By keeping under control finite element discretization errors, it is possible to focus on constitutive modelling and its effect on the structural response. As illustrated with the single-edge notched beam test, the proposed approach allows to assess the influence of the particular choice of the state variable, the evolution law for damage or the material parameters in a reliable manner. In particular, the capability of the Mazars model to capture the curved crack pattern observed in experiments – a debated issue in the literature – has been confirmed.

Various interesting topics lie ahead. As already discussed, work is under progress to develop an error estimation procedure that takes fully into account the nonlocal interaction. The basic idea is that the error associated to the nonlocal interaction between different elements can be cast as a pollution error. Also in perspective is goal-oriented error estimation: instead of estimating the error of the displacement field, it may be preferable to estimate the error in outputs of special relevance, such as the peak load in the Brazilian test.

On a wider scope, a combined experimental-numerical study could now be used to identify the material parameters for the nonlocal damage models. If this process is done without controlling the quality of the FE solution, the obtained parameters fit a solution affected by discretization errors, so their significance is limited.

References

Arroyo, M., Díez, P., Huerta, A., 1997. Error estimation and adaptivity in strain localisation problems with softening materials. Monograph no. 40, International Center for Numerical Methods in Engineering, Barcelona.

Askes, H., Sluys, L.J., 1999. Remeshing strategies for adaptive ALE analysis of strain localisation. European Journal of Mechanics A/Solids 19, 447–467.

Bažant, Z.P., Belytschko, T., Chang, T.P., 1984. Continuum theory for strain softening. Journal of Engineering Mechanics 110, 1666–1692.

Bažant, Z.P., Pijaudier-Cabot, G., 1988. Nonlocal continuum damage, localization instability and convergence. ASME Journal of Applied Mechanics 55, 287–293.

Carmona, S., Gettu, R., Aguado, A., 1998. Study of the post-peak behavior of concrete in the splitting-tension test. Fracture Mechanics of Concrete Structures (Proceedings of FRAMCOS-3). AEDIFICATIO Publishers, Freiburg, pp. 111–120.

Carpinteri, A., Valente, S., Ferrara, G., Melchiorri, G., 1993. Is mode II fracture energy a real material property. Computers and Structures 48, 397–413.

Castro-Montero, A., Jia, Z., Shah, S.P., 1995. Evaluation of damage in Brazilian test using holographic interferometry. ACI Materials Journal 92, 268–275.

Crisfield, M.A., 1991. Non-linear finite element analysis of solids and structures. Vol. 1, Essentials. Wiley, Chichester.

de Borst, R., Pamin, J., Peerlings, R.H.J., Sluys, L.J., 1995. On gradient-enhanced damage and plasticity models for failure in quasi-brittle and frictional materials. Computational Mechanics 17, 130–141.

de Borst, R., Sluys, L.J., Mülhaus, H.-B., Pamin, J., 1993. Fundamental issues in finite element analysis of localization of deformation. Engineering Computations 10, 99–121.

Vree, J.H.P., Brekelmans, W.A.M., Gils, M.A.J., 1995. Comparison of nonlocal approaches in continuum damage mechanics. Computers and Structures 55, 581–588.

Díez, P., Arroyo, M., Huerta, A., 2000. Adaptivity based on error estimation for viscoplastic softening materials. Mechanics of Cohesive-Frictional Materials 5, 87–112.

Díez, P., Egozcue, J.J., Huerta, A., 1998a. A posteriori error estimation for standard finite element analysis. Computer Methods in Applied Mechanics and Engineering 163, 141–157.

Díez, P., Egozcue, J.J., Huerta, A., 1998b. Analysis of the average efficiency of an error estimator. In: Křížek, M., et al. (Eds.), Finite Element Methods: Superconvergence, Post-Processing and a Posteriori Estimates, Marcel Dekker, New York, pp. 113–126.

Díez, P., Huerta, A., 1999. A unified approach to remeshing strategies for finite element *h*-adaptivity. Computer Methods in Applied Mechanics and Engineering 176, 215–229.

Fichant, S., La Borderie, C., Pijaudier-Cabot, G., 1999. Isotropic and anisotropic descriptions of damage in concrete structures. Mechanics of Cohesive-Frictional Materials 4, 339–359.

Geers, M.G.D., 1999. A unification of path following techniques for nonlinear finite element analysis. Proceedings of the European Conference on Computational Mechanics 1999 (in CD-ROM), Munich.

Huerta, A., Díez, P., Arroyo, M., 1997. An a posteriori error estimator with global (pollution) information applied to a regularized localization problem. Proceedings of the McNU'97 Joint ASME-ASCE-SES Summer Meeting, Evanston, Illinois.

Huerta, A., Díez, P., Egozcue, J.J., 1998. Error estimation for linear and nonlinear problems. In: Křížek, M., et al. (Eds.), Finite Element Methods: Superconvergence, Post-Processing and a Posteriori Estimates, Marcel Dekker, New York, pp. 183–194.

Huerta, A., Díez, P., 2000. Error estimation including pollution assessment for nonlinear finite element analysis. Computer Methods and Applied Mechanics in Engineering 181, 21–41.

Huerta, A., Pijaudier-Cabot, G., 1994. Discretization influence on regularization by two localization limiters. Journal of Engineering Mechanics 120, 1198–1218.

Huerta, A., Rodríguez-Ferran, A., Díez, P., Sarrate, J., 1999. Adaptive finite element strategies based on error assessment. International Journal for Numerical Methods in Engineering 46, 1803–1818.

Jirásek, M., 1999. Computational aspects of nonlocal models. Proceedings of the European Conference on Computational Mechanics 1999 (in CD-ROM), Munich.

Lemaitre, J., Chaboche, J.-L., 1990. Mechanics of Solid Materials. Cambridge University Press, Cambridge.

Mazars, J., 1986. A description of micro- and macro-scale damage of concrete structures. Journal of Engineering Fracture Mechanics 25, 729–737.

Mazars, J., Pijaudier-Cabot, G., 1989. Continuum damage theory: application to concrete. ASCE Journal of Engineering Mechanics 115, 345–365.

Peerlings, R.H.J., de Borst, R., Brekelmans, W.A.M., Geers, M.G.D., 1998. Gradient-enhanced damage modelling of concrete fracture. Mechanics of Cohesive-Frictional Materials 3, 323–342.

Pegon, P., Anthoine, A., 1994. Numerical strategies for solving continuum damage problems involving softening: application to the homogenization of masonry. Proceedings of the Second International Conference on Computational Structures Technology, Athens.

Pijaudier-Cabot, G., 1996. Damage based models. Lecture Notes of the Summer Course on Mechanics of Concrete, Janovice–Cracow, Poland.

Pijaudier-Cabot, G., Bažant, Z.P., 1987. Nonlocal damage theory. Journal of Engineering Mechanics 118, 1512–1533.

Pijaudier-Cabot, G., Huerta, A., 1991. Finite element analysis of bifurcation in nonlocal strain softening solids. Computer Methods in Applied Mechanics and Engineering 90, 905–919.

Pijaudier-Cabot, G., Mazars, J., 1991. Steel-concrete bond analysis with nonlocal continuous damage. Journal of Structural Engineering 117, 862–882.

Rocco, C., Guinea, G.V., Planas, J., Elices, M., 1999. Mechanisms of rupture in splitting tests. ACI Materials Journal 96, 52–60.

Sarrate, J., Huerta, A., 2000. Efficient unstructured quadrilateral mesh generation. International Journal for Numerical Methods in Engineering, in press.

Schlangen, E., 1993. Experimental and numerical analysis of fracture processes in concrete. Dissertation, Delft University of Technology.